Biosensors and Bioelectronics 126 (2019) 96–101

Contents lists available at ScienceDirect

Biosensors and Bioelectronics

journal homepage: www.elsevier.com/locate/bios

Cationic cyanine chromophore-assembled upconversion nanoparticles for sensing and imaging H_2S in living cells and zebrafish

Fangfang Wang, Cuiling Zhang*, Xuetong Qu, Shasha Cheng, Yuezhong Xian*

Shanghai Key Laboratory of Green Chemistry and Chemical Processes, Department of Chemistry, School of Chemistry and Molecular Engineering, East China Normal University, Shanghai 200241, China

ARTICLE INFO

Keywords:
Hydrogen sulfide (H_2S)
Turn-on fluorescent probe
Chromophore
Upconversion nanoparticles
Bioimaging

ABSTRACT

Elevated hydrogen sulfide (H_2S) level is closely associated with various diseases. So the sensing of H_2S is noteworthy for divulging its role in diagnosing these diseases. Herein, we proposed poly(acrylic acid)-modified upconversion nanoparticles assembled with cationic near-infrared cyanine chromophores (Cy7-Cl) as the nanoprobe (Cy7-UCNPs) for monitoring H_2S based on thiolation reactions. The presence of H_2S resulted into about five-fold enhancement in the luminescence intensity of Cy7-UCNPs and the nanoprobe showed a good linearity (R^2 = 0.9952) over the range of 1.0 − 90 μM. Furthermore, Cy7-UCNPs were successfully employed in sensing and imaging of exogenous and endogenous H_2S in live cells and zebrafish. The system shows great potential in the field of nanobiomedicine because of the many excellent properties including high sensitivity, good selectivity, and low cytotoxicity.

1. Introduction

Hydrogen sulfide (H_2S), a toxic gas signal molecule, is linked to human health and physiology. Aberrant levels of endogenous H_2S is closely related to many diseases in the neuronal, gastrointestinal, circulatory, and endocrine systems, such as colorectal, ovarian, and breast cancers (Hartle and Pluth, 2016; Xu et al., 2018). Hence, H_2S can be regarded as a biomarker for the diagnosis and therapeutic target for these diseases. Undoubtedly, all the functions of H_2S call for a rapid and simple strategy for the detection of the gaseous molecule to guarantee human health.

Several methods have been developed to determine H_2S, such as electrochemistry (Xu et al., 2016), electrochemiluminescence (Yue et al., 2015), bioluminescence (Ke et al., 2016), fluorometry (Bai et al., 2018; Chen et al., 2016; Hai et al., 2015; Kim et al., 2017; Li et al., 2015; Lippert et al., 2011; Liu et al., 2016; Peng et al., 2016; Wang et al., 2018, 2017), colorimetry (Chen et al., 2018; Jia et al., 2017; Zeng et al., 2018; Zhang et al., 2017b), and surface-enhanced Raman scattering (Prado et al., 2015). Among them, fluorescent assay is regarded as one of the most hopeful approaches because of the good selectivity, high sensitivity, and real-time virtues. So far, a wide variety of fluorescent H_2S probes have been constructed. Recently, organic molecule fluorescent probes have been utilized in the detection of H_2S owing to their sensitivity and adaptability. For example, Peng' group developed a ratiometric near-infrared (NIR) fluorescent probe with excellent enhancement, large emission shift, and fast response for the sensitive detection of H_2S (Li et al., 2015). Chang et al. reported fluorescent probes (sulfidefluor-1 and sulfidefluor-2) based on reaction for the imaging of H_2S in living cells (Lippert et al., 2011). Tan and co-workers designed a two-photon-excited supramolecular fluorescent nanoplatform for accurate determination of H_2S with good selectivity and high sensitivity (Wang et al., 2017). Although many progresses have been achieved for fluorescent detection of H_2S, several challenges are still present, (1) biothiols can interfere the determination of H_2S because of the non-specificity of luminescence probes, (2) traditional organic fluorophores probes usually suffer from poor water solubility and underlying photobleaching, (3) for real biosamples, the autofluorescence produced by proteins and peptides also impairs the signal-to-noise ratio. Therefore, in order to solve the above-mentioned problems, it is of great significance to develop new H_2S probes with high sensitivity and selectivity for biological systems.

Compared to organic fluorescent probes, lanthanide-doped upconversion nanoparticles (UCNPs) have many interesting characteristics, such as zero autofluorescence background, high photostability, no blinking, large anti-Stokes shift up to hundreds of nanometers, high signal-to-noise ratio and penetration depth (Chen et al., 2015; Yang et al., 2015; Zheng et al., 2015). So UCNPs-based probes for living cells and in vivo imaging have attracted considerable attentions (Chen et al.,

* Corresponding authors.
E-mail addresses: clzhang@chem.ecnu.edu.cn (C. Zhang), yzxian@chem.ecnu.edu.cn (Y. Xian).

https://doi.org/10.1016/j.bios.2018.10.056
Received 1 September 2018; Received in revised form 11 October 2018; Accepted 25 October 2018
Available online 27 October 2018
0956-5663/

2015; Gu and Zhang, 2018; Liu et al., 2018; Zheng et al., 2015). On the other side, organic chromophores with specific recognition ability have been commonly utilized in highly selective detecting applications. Based on these findings, several bybrid systems composed of organic chromophores and UCNPs on the basis of the significant imaging capacity from UCNPs and outstanding recognition properties of chromophores have been reported to detect H_2S. For example, Loo et al. have successfully used organic optical sensor-attached UCNPs as detection probes to sense and bioimage H_2S for the first time (Zhou et al., 2014). Chang' group have developed a sensing platform using dye assembled with UCNPs for H_2S detection in live cells and in blood serum (Peng et al., 2016). However, in the above study, core-only nanoparticles have the limitation of low luminescence efficiency due to surface-related quenching (Chen et al., 2014). The surface quenching effect needs an inert shell to diminish energy loss and enhance luminescence efficiency (Li et al., 2014). Therefore, the construction of core–shell UCNPs is more beneficial to biological applications. Meanwhile, detection signals of them were visible light and the syntheses of organic chromophores were very tedious. Based on the above facts, we have developed a H_2S sensing platform with the features of NIR excitation and NIR emission by integrating the commercial NIR dye onto core–shell UCNPs.

Herein, the nanoassembly of poly(acrylic acid)-modified UCNPs (PAA-UCNPs) with H_2S-responsive cationic NIR cyanine chromophores (Cy7-Cl) (named as Cy7-UCNPs) was developed for highly sensitive and selective detection of H_2S with broad liner range and fast response. Upon reacting with H_2S via nucleophilic thiolation (Wu et al., 2014b), the nanoprobe generated concentration-dependent, turn-on NIR emission at 800 nm with the excitation wavelength of 980 nm, therefore, it can be used to detect and bioimage H_2S in vitro and in vivo. Fig. 1A shows the schematic illustration for fluorescent H_2S detection, PAA-UCNPs were employed as energy donor and NIR absorbing chromophore H_2S-responsive Cy7-Cl was used as the energy acceptor. Without H_2S, Cy7-UCNPs show weak luminescence at 800 nm because of an efficient energy transfer (ET) from PAA-UCNPs to Cy7-Cl (Fig. 1B). However, in the presence of Na_2S (a commonly employed H_2S donor), the occurrence of the highly selective reaction between Cy7-Cl and H_2S blocks the absorption of the luminescence emission from PAA-UCNPs (Fig. 1C). Therefore, H_2S introduction results in the turn-on luminescence of UCNPs at 800 nm concomitantly. Compared with the turn-off fluorescent probes, the turn-on probe has a positive signal readout with good spatial resolution on a dark background. Moreover, the Cy7-UCNPs nanoassembly includes NIR excitation (980 nm) and NIR emission (around 800 nm). These features are beneficial for biosensing and bioimaging due to high penetration depth and low auto-fluorescence background, especially, under in vivo conditions.

2. Material and methods

Details on chemicals, materials, apparatus and experiment procedures used in this work can be found in the Supplementary Information.

3. Results and discussion

3.1. Synthesis and characterization

XRD and TEM techniques were employed to investigate the phase and morphology of UCNPs. The XRD patterns of UCNPs were shown in Fig. 2A, and all the diffraction peaks matched well with standard

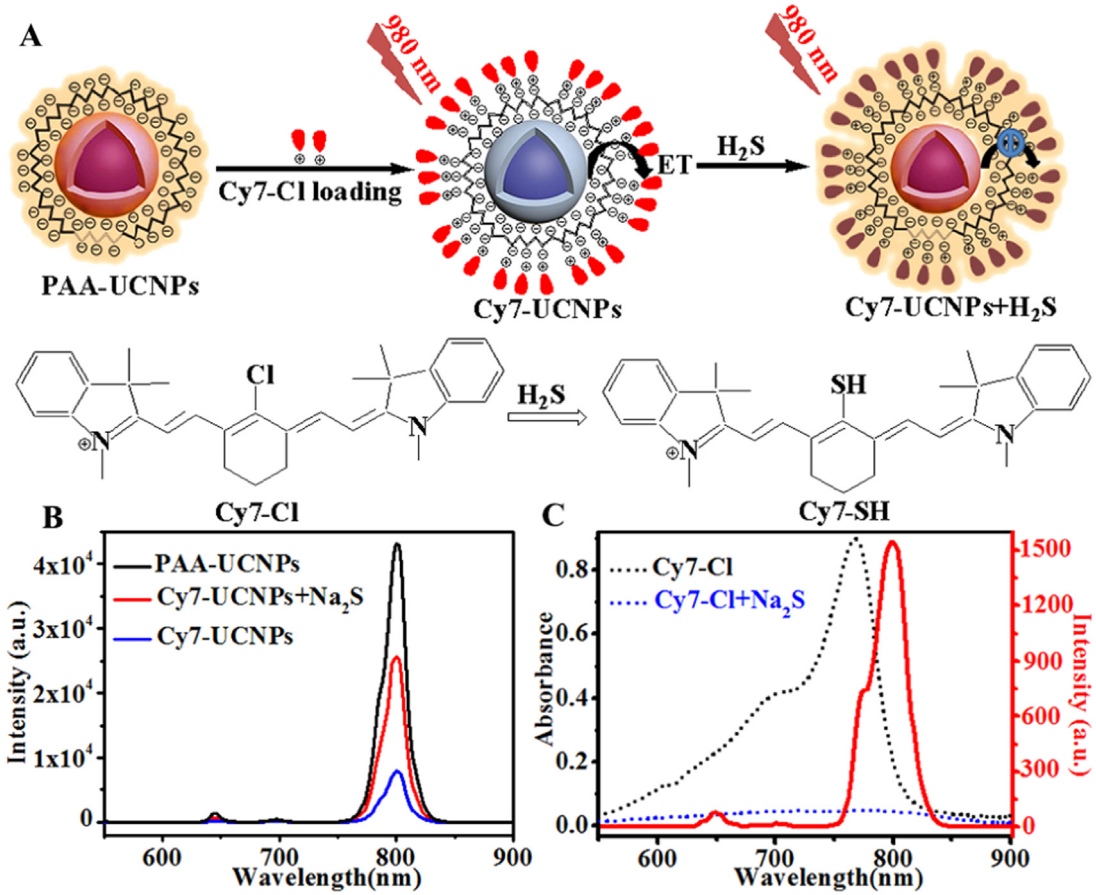

Fig. 1. (A) Schematic illustration of luminescence system based on the Cy7-UCNPs nanoassembly for H_2S detection. (B) Luminescence spectra of 0.1 mg/mL PAA-UCNPs, Cy7-UCNPs with and without 50 μM Na_2S. (C) Luminescence spectrum (red line) of UCNPs (λ_{ex} = 980 nm) and UV–vis absorption spectra of Cy7-Cl with (blue line) and without (black line) Na_2S.

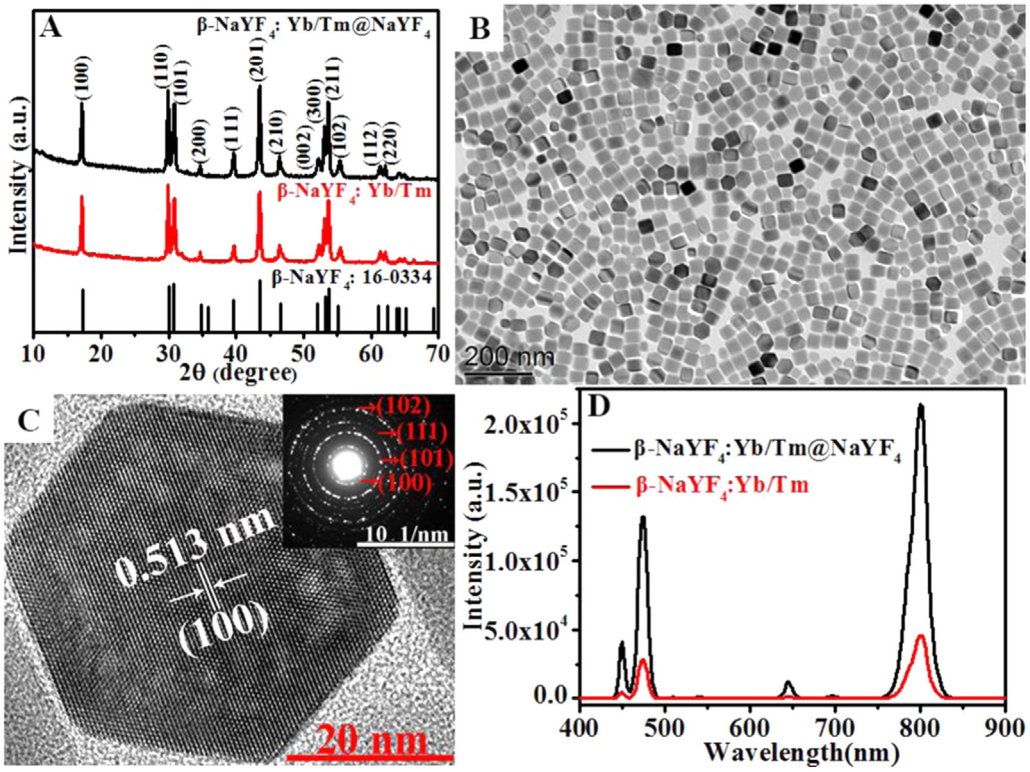

Fig. 2. (A) XRD patterns of the as-synthesized core and core−shell nanoparticles. (B) TEM and (C) HRTEM images (inset is the SAED pattern) of the core−shell nanoparticles. (D) Upconversion luminescence spectra of the core and core−shell nanoparticles (λ_{ex} = 980 nm).

pattern of hexagonal $NaYF_4$ [JCPDS card No. 16–0334]. As presented in Fig. 2B, UCNPs were uniform polyhedrons. Compared with the TEM image of the core nanoparticles (Fig. S1), the resulting core-shell nanoparticles show obvious increase of the particle size from 11.27 to 44.6 nm (Fig. S2). Additionally, the results of element mapping (Fig. S3) and lifetime for core and core-shell nanoparticles (Fig. S4) indicate the covering of inert shell over the surface of core. Yb element was distributed in the core while Na, Y, and F were distributed in the core and shell. The existence of Tm was also observed. The measured lattice distance (0.513 nm) from the HRTEM image (Fig. 2C) is consistent with the (100) plane of the hexagonal $NaYF_4$ phase, demonstrating highly crystalline nature of the as-prepared UCNPs. The diffraction rings in corresponding SAED pattern reveal that the UCNPs are polycrystalline in nature. From inside to outside, the rings can be indexed to (100), (101), (111), and (102) planes of $NaYF_4$, respectively. Notably, the existence of shell structure can efficiently enhance the luminescence of the UCNPs due to the prevention of the lanthanide activators from environmental quenching (Fig. 2D). The fluorescence intensities indicate ~5 times enhancement for core-shell structured UCNPs.

To ensure the assembly of Cy7-Cl with UCNPs, we removed the OA ligands from UCNPs by acid treatment and further coated with PAA in order to improve their water solubility. The positively charged Cy7-Cl was then assembled onto the surface of the UCNPs by electrostatic attraction. It was noteworthy that the morphology of UCNPs assembly with Cy7-Cl was almost the same as that of PAA-UCNPs (Fig. S5), which might ascribe to the assembly with small molecule dye. Zeta potential for ligand-free UCNPs, PAA-UCNPs and Cy7-UCNPs were about + 32.1, − 24.3 and 29.9 mV, respectively (Fig. S6), indicating the successful PAA coating and assembling of chromophore with UCNPs. The presence of PAA on the surface of UCNPs was also proved by FTIR spectroscopy. The peaks in Fig. S7 at about 1245 cm^{-1} and 1721 cm^{-1} denoted the existence of C-O and C=O stretching modes (Zhang et al., 2017b, 2013). FTIR spectra and zeta potential confirm the successful assembly of Cy7-Cl to the surface of the PAA-UCNPs. Upon successful assembly of Cy7-Cl, the resulting colloidal solution was green and its NIR emission around 800 nm was significantly weakened with the increment of Cy7-Cl concentration (Fig. S8). We also discovered that the emission lifetime of the prepared nanoprobes at 800 nm was reduced from 1.749 to 1.335 ms after Cy7-Cl assembling (Fig. S9). It indicated the assembly of Cy7-Cl with PAA-UCNPs led to the efficient ET from PAA-UCNPs to Cy7-Cl. The efficiency of förster resonance energy transfer (FRET) process was calculated by the following formula,

$$E = 1 - \frac{\tau_{DA}}{\tau_D}$$

where τ_{DA} and τ_D are the donor lifetime with and without the acceptor (Bednarkiewicz et al., 2010; Peng et al., 2016). Based on the results of the lifetime for PAA-UCNPs at 800 nm before and after assembling with Cy7-Cl, the FRET efficiency between PAA-UCNPs and Cy7-Cl is about 23.7%. The luminescence lifetime and intensities decrease denotes that the luminescence quenching occurs through FRET and emission-reabsorption (Peng et al., 2017, 2016; Wu et al., 2014a).

3.2. Response of Cy7-UCNPs to H_2S

For maximum quenching of UCNPs luminescence, the highest Cy7-Cl loading amount on PAA-UCNPs was investigated. Based on the absorption spectra of Cy7-Cl, the loading amount of Cy7-Cl on the surface of UCNPs was about 17.9 μM with regard to colloidal PAA-UCNPs with the concentration of 0.1 mg/mL, which was about 7.97 wt% of Cy7-UCNPs (Fig. S10). Under optimized condition, more than 75% of the original luminescence of PAA-UCNPs was quenched. The optical response of Cy7-UCNPs toward H_2S was further studied in PBS. The treatment of Cy7-UCNPs with Na_2S induced the robust increase of the emission at 800 nm, and reached a plateau within 10 min, which provided a versatile strategy for the monitoring of H_2S-related biological processes. Notably, Cy7-UCNPs showed good photostability in aqueous solution (Fig. S11) under the illumination of 980 nm. Almost no luminescence changes were observed under continuous irradiation for 1 h.

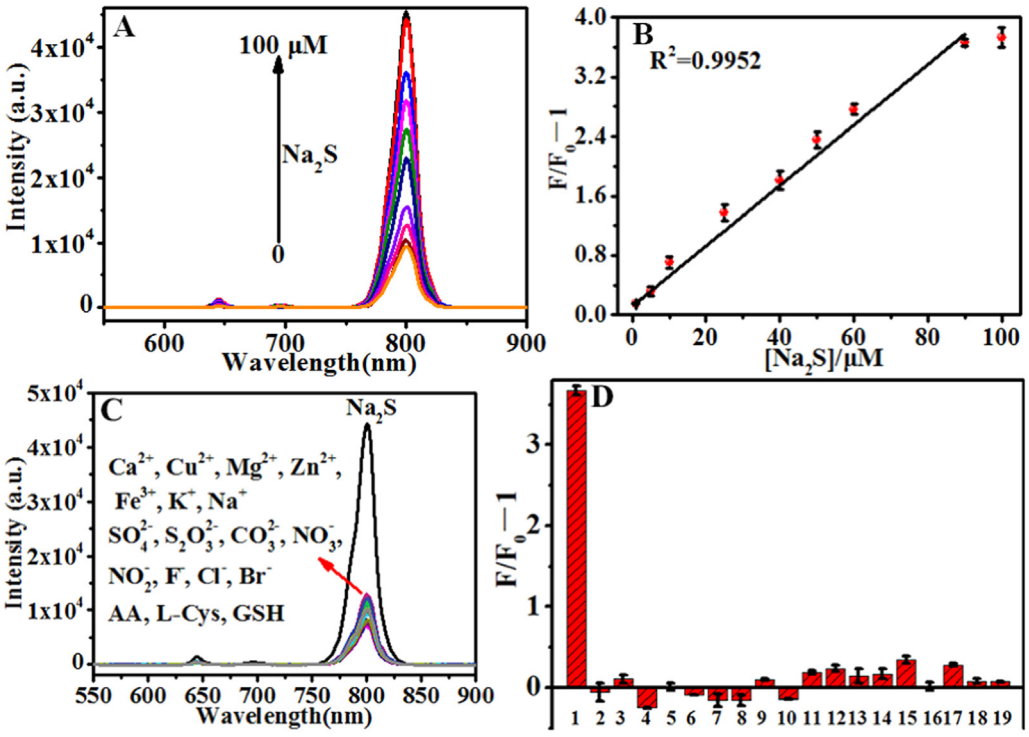

Fig. 3. (A) Upconversion luminescence response of 100 μg/mL Cy7-UCNPs in PBS against Na_2S concentration (0–100 μM). (B) The fluorescence change ratio (F/F_0 - 1) at 800 nm versus Na_2S concentration. F_0 and F represent the emission intensity of Cy7-UCNPs before and after adding Na_2S, respectively. (C) Luminescence spectra of 0.1 mg/mL Cy7-UCNPs with Na_2S and other interference. (D) Selectivity of the fluorescent probe for H_2S. 1, Na_2S, 2, Ca^{2+}, 3, Cu^{2+}, 4, Fe^{3+}, 5, Mg^{2+}, 6, Zn^{2+}, 7, K^+, 8, Na^+, 9, SO_4^{2-}, 10, $S_2O_3^{2-}$, 11, CO_3^{2-}, 12, NO_3^-, 13, NO_2^-, 14, F^-, 15, Cl^-, 16, Br^-, 17, AA, 18, L-Cys, 19, GSH; [Na_2S] = 90 μM; [interference substances] = 500 μM.

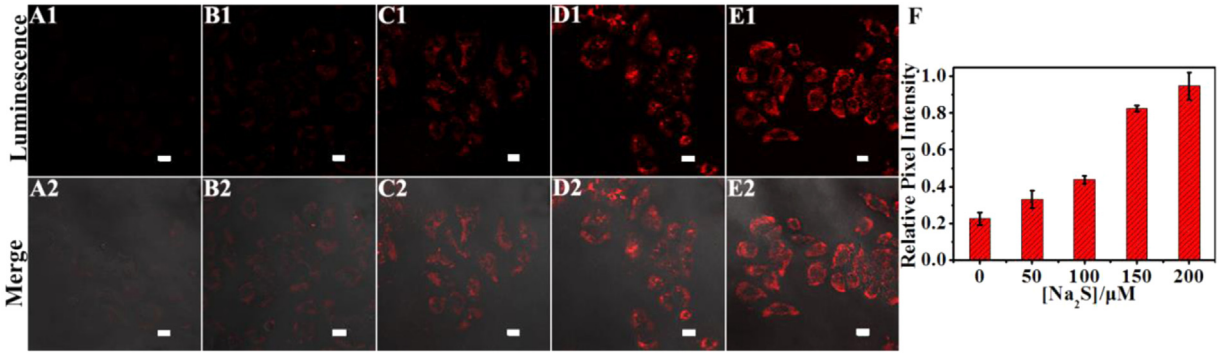

Fig. 4. Luminescence images of Hela cells cultured with Cy7-UCNPs and different amounts of Na_2S. (A) 0, (B) 50, (C) 100, (D) 150, (E) 200 μM. (F) Relationship between the mean luminescence intensity and the increased concentration of Na_2S in A-E correspondingly. Scale bar is 20 μm.

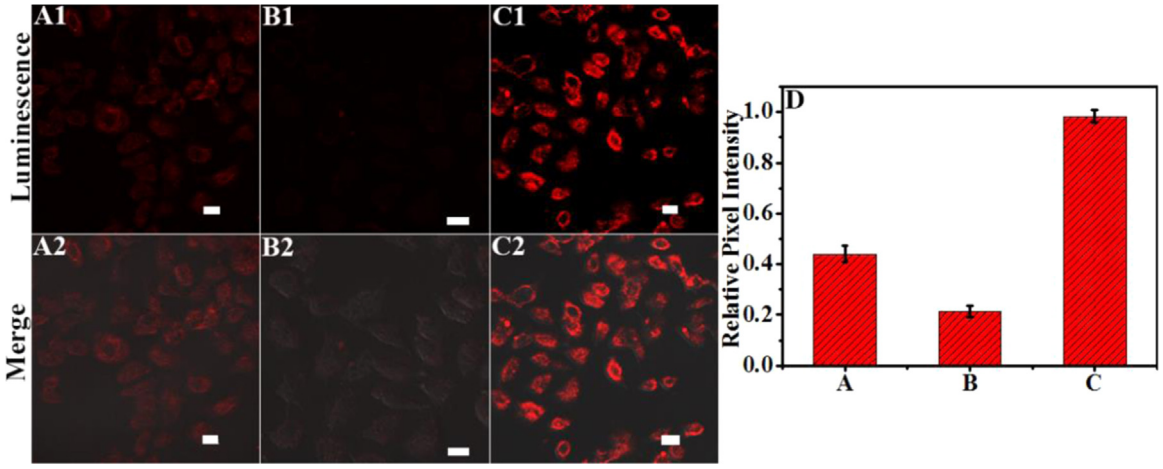

Fig. 5. Luminescence bioimage of H_2S in MCF-7 cells. (A) MCF-7 cells were incubated with Cy7-UCNPs for 6 h. (B) MCF-7 cells were pretreated with NMM for 0.5 h, followed by incubation with Cy7-UCNPs for 6 h. (C) MCF-7 cells were pretreated with L-Cys for 0.5 h and then Cy7-UCNPs for 6 h. (D) The corresponding average luminescence intensity for A-C. Scale bar = 20 μm.

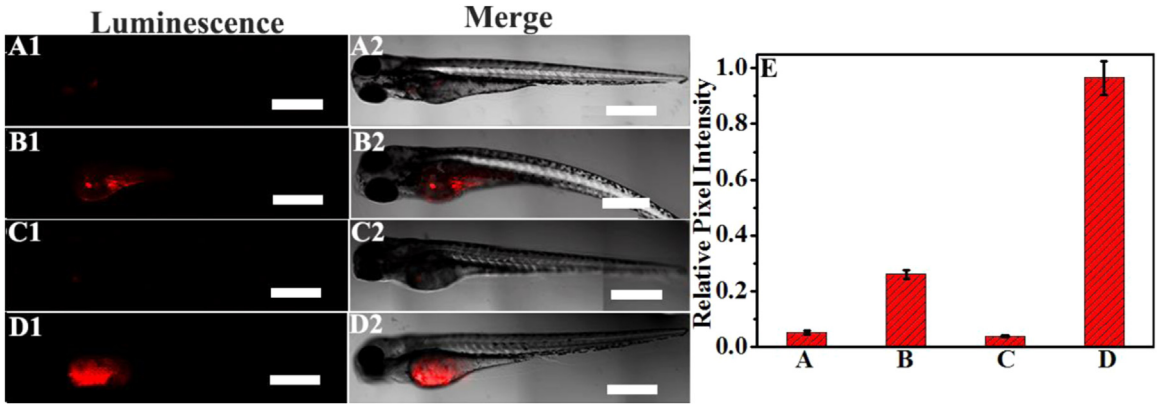

Fig. 6. Representative luminescence images of H_2S in zebrafish using Cy7-UCNPs as nanoprobes. (A) The normal zebrafish was microinjected with PBS buffer and then nanoprobes after 30 min (B) The tumor-bearing zebrafish was microinjected with PBS buffer firstly and then nanoprobes after 30 min (C) The tumor-bearing zebrafish was pretreated with NMM for 30 min and then microinjected with nanoprobes. (D) The tumor-bearing zebrafish pretreated with L-Cys for 30 min was microinjected with nanoprobes. (E) The corresponding average luminescence intensity for A-D (n = 5). Scale bar = 500 μm.

With the gradual increase the concentration of Na_2S, the luminescence intensity at 800 nm was boosted due to the significant hypochromicity for the absorption of Cy7-Cl (Fig. S12). The nanoassembly shows a good linearity over the range of 1–90 μM for H_2S measurement (Fig. 3A-B). The limit of detection (LOD) of H_2S is about 510 nM, which is comparable to that of the recently reported H_2S probes (Table S1) (Bai et al., 2018; Chen et al., 2016; Hai et al., 2015; Kim et al., 2017; Li et al., 2015; Peng et al., 2016; Wang et al., 2018, 2017; Zhang et al., 2017a), indicating the high sensitivity of Cy7-UCNPs for detection of H_2S.

To evaluate the selectivity of the probe Cy7-UCNPs, we selected a variety of potential interferences, including metal ions (Ca^{2+}, Cu^{2+}, Fe^{3+}, Mg^{2+}, Zn^{2+}, K^+, Na^+), anions (SO_4^{2-}, $S_2O_3^{2-}$, CO_3^{2-}, NO_3^-, NO_2^-, F^-, Cl^-, Br^-), and some biological species (Cys, GSH, AA). As shown in Fig. 3C-D, these species caused negligible changes in luminescence, whereas the introduction of Na_2S led to a significant enhancement in luminescence intensity. In addition, only Na_2S resulted in a sharp decrease of the absorption of Cy7-UCNPs (Fig. S13), further indicating the highly selective recognition ability. These results show that our developed method can be further applied in biological system without the interference from coexisting substances, even for other sulfur-containing species.

3.3. Imaging H_2S in living cells

To validate the biological application, we first used CCK-8 assay to evaluate the cytotoxicity of Cy7-UCNPs and PAA-UCNPs. In our study, HeLa cells were selected as model for exogenous H_2S bioimaging. The cells viability were higher than 90% even the dose of the nanoprobe is up to 240 μg/mL (Fig. S14), suggesting that Cy7-UCNPs have good biocompatibility. After incubated with 200 μg/mL Cy7-UCNPs for 6 h, the bioimaging was performed under a CLSM. As shown in Fig. 4A, HeLa cells incubated with Cy7-UCNPs only showed very weak NIR emission. After the addition of Na_2S into the HeLa cells with Cy7-UCNPs and further incubated for 30 min, we can observe that the luminescence intensity for the cells is gradually enhanced along with the augmentation of Na_2S concentration from 0 to 200 μM (Fig. 4B-E). The average luminescence intensity was further analyzed via Nikon software and shown in Fig. 4F. The experimental results demonstrate that Cy7-UCNPs are suitable for bioimaging of exogenous H_2S in living cells.

Endogenous H_2S is mainly produced from cysteine or cysteine derivatives catalyzed by cystathionine β-synthase (CBS) and cystathionine γ-lyase (CSE) (Hartle and Pluth, 2016; Zhang et al., 2017b), and the MCF-7 cells can express high levels of CBS and CSE (Li et al., 2015; Xiong et al., 2018; Xu et al., 2018). Therefore, MCF-7 cells were selected as the model for endogenous H_2S bioimaing. As shown in Fig. S15, Cy7-UCNPs show the low cytotoxicity. In contrast with HeLa cells, stable and bright luminescence signals were observed MCF-7 cells in the NIR channel, which were also incubated with Cy7-UCNPs for 6 h (Fig. 5A). It indicates that MCF-7 cells can produce endogenous H_2S due to the expression of CBS and CSE. As for Fig. 5B, the MCF-7 cells were treated with NMM for 0.5 h and then incubated with Cy7-UCNPs for 6 h, we can not observe obvious NIR emission. It was reported that NMM was a scavenger for intracellular H_2S (Li et al., 2015), therefore, the treatment of the MCF-7 cells led to the removal of H_2S and disappearance of NIR signal. On the contrary, if the MCF-7 cells were firstly handled with L-Cys and then cultured with Cy7-UCNPs for 6 h, an obvious enhancement of NIR emission was observed (Fig. 5C). It is because that L-Cys is the precursor of H_2S and can be converted into H_2S in the presence of CBS and CSE. Fig. 5D shows the corresponding average luminescence intensity for Fig. 5A-C. These results demonstrate the feasibility of Cy7-UCNPs for the endogenous H_2S bioimaging in biological systems.

3.4. Luminescence imaging of H_2S in zebrafish

We further evaluated the in vivo metabolism process of Cy7-UCNPs in zebrafish pretreated with L-Cys. As shown in Fig. S16, it can be observed that the Cy7-UCNPs microinjected into the tumor regions were metabolized completely within 5 h. As shown in Fig. 6B, it is found that tumor-bearing zebrafish pretreated with PBS buffer and microinjected with Cy7-UCNPs emits stronger NIR luminescence signal than that of normal zebrafish (Fig. 6A). In contrast, the tumor-bearing zebrafish treated with NMM and Cy7-UCNPs displays no noticeable NIR luminescence (Fig. 6C). Furthermore, a remarkably robust luminescence signal is observed for the tumor-bearing zebrafish treated with L-Cys and Cy7-UCNPs (Fig. 6D). These results indicate that the nanoassembly of Cy7-UCNPs is capable of distinguishing normal and tumor-bearing zebrafish through in vivo imaging due to the excellent feature of NIR excitation and NIR emission. It show the great potential for diagnosis of H_2S-related diseases.

4. Conclusions

In summary, we have developed a H_2S sensing platform using Cy7-Cl assembled with UCNPs. The powerful strategy that integrates the chromophores onto UCNPs shows specific luminescence response to H_2S with the features of NIR excitation and NIR emission. Furthermore, the nanoprobes exhibit rapid response, high sensitivity, and excellent selectivity, especially, for the mercaptans in physiological system. Incorporation the benefits of specific recognition by Cy7-Cl and the fascinating photophysical properties of PAA-UCNPs, we successfully

demonstrate that Cy7-UCNPs are suitable for H_2S detection and bioimaging in biosystem. The advantages of the nanoprobes make Cy7-UCNPs to be a potential tool for further diagnosis of H_2S-related diseases in clinical.

Acknowledgements

This work was financially supported from the National Key R&D Program of China (2018YFF0215404), Shanghai Natural Science Foundation (18ZR1411300), National Natural Science Foundation of China (21605050, 11727810), and the Postdoctoral Science Foundation of China (2018T110367).

Appendix A. Supplementary material

Supplementary data associated with this article can be found in the online version at doi:10.1016/j.bios.2018.10.056.

References

Bednarkiewicz, A., Nyk, M., Samoc, M., Strek, W., 2010. J. Phys. Chem. C 114, 17535–17541.
Bai, X.L., Xu, S.Y., Wang, L.Y., 2018. Anal. Chem. 90, 3270–3275.
Chen, G.Y., Ågren, H., Ohulchanskyy, T.Y., Prasad, P.N., 2015. Chem. Soc. Rev. 44, 1680–1713.
Chen, G.Y., Qiu, H.L., Prasad, P.N., Chen, X.Y., 2014. Chem. Rev. 114, 5161–5214.
Chen, P.C., Li, Y.C., Ma, J.Y., Huang, J.Y., Chen, C.F., Chang, H.T., 2016. Sci. Rep. 6, 24882.
Chen, Z.H., Chen, C.Q., Huang, H.W., Luo, F., Guo, L.H., Zhang, L., Lin, Z.Y., Chen, G.N., 2018. Anal. Chem. 90, 6222–6228.
Gu, B., Zhang, Q.C., 2018. Adv. Sci. 5, 1700609.
Hai, Z.J., Bao, Y.J., Miao, Q.Q., Yi, X.Y., Liang, G.L., 2015. Anal. Chem. 87, 2678–2684.
Hartle, M.D., Pluth, M.D., 2016. Chem. Soc. Rev. 45, 6108–6117.
Jia, Y.X., Guo, Y.M., Wang, S.W., Chen, W.W., Zhang, J.J., Zheng, W.S., Jiang, X.Y., 2017. Nanoscale 9, 9811–9817.
Ke, B.W., Wu, W.X., Liu, W., Liang, H., Gong, D.Y., Hu, X.T., Li, M.Y., 2016. Anal. Chem. 88, 592–595.
Kim, M., Seo, Y.H., Kim, Y., Heo, J., Jang, W.D., Sim, S.J., Kim, S., 2017. Chem. Commun. 53, 2275–2278.
Li, H.D., Yao, Q.C., Fan, J.L., Jiang, N., Wang, J.Y., Xia, J., Peng, X.J., 2015. Chem. Commun. 51, 16225–16228.
Li, X.M., Wang, R., Zhang, F., Zhao, D.Y., 2014. Nano Lett. 14, 3634–3639.
Lippert, A.R., New, E.J., Chang, C.J., 2011. J. Am. Chem. Soc. 133, 10078–10080.
Liu, J., Guo, X.D., Hu, R., Liu, X.Y., Wang, S.Q., Li, S.Y., Li, Y., Yang, G.Q., 2016. Anal. Chem. 88, 1052–1057.
Liu, Y.X., Jiang, A.Q., Jia, Q., Zhai, X.J., Liu, L.D., Ma, L.Y., Zhou, J., 2018. Chem. Sci. 9, 5242–5251.
Peng, J.J., Samanta, A., Zeng, X., Han, S.Y., Wang, L., Su, D.D., Loong, D.T.B., Kang, N.Y., Park, S.J., All, A.H., Jiang, W.X., Yuan, L., Liu, X.G., Chang, Y.T., 2017. Angew. Chem. Int. Ed. 56, 4165–4169.
Peng, J.J., Teoh, C.L., Zeng, X., Samanta, A., Wang, L., Xu, W., Su, D.D., Yuan, L., Liu, X.G., Chang, Y.T., 2016. Adv. Funct. Mater. 26, 191–199.
Prado, A.R., Oliveira, J.P., Pereira, R.H.A., Guimarães, M.C.C., Nogueira, B.V., Castro, E.V.R., Almeida, L.C.P., Ribeiro, M.R.N., Pontes, M.J., 2015. Plasmonics 10, 1097–1103.
Wang, F.Y., Xu, G., Gu, X.F., Wang, Z.J., Wang, Z.Q., Shi, B., Lu, C.F., Gong, X.Q., Zhao, C.C., 2018. Biomaterials 159, 82–90.
Wang, P., Zhang, C., Liu, H.W., Xiong, M.Y., Yin, S.Y., Yang, Y., Hu, X.X., Yin, X., Zhang, X.B., Tan, W.H., 2017. Chem. Sci. 8, 8214–8220.
Wu, T.Q., Wilson, D., Branda, N.R., 2014a. Chem. Mater. 26, 4313–4320.
Wu, X.J., Shi, J.Q., Yang, L., Han, J.H., Han, S., 2014b. Bioorg. Med. Chem. Lett. 24, 314–316.
Xiong, J.C., Xia, L.L., Huang, Q.L., Huang, J.X., Gu, Y.Q., Wang, P., 2018. Talanta 184, 109–114.
Xu, G., Yan, Q.L., Lv, X.G., Zhu, Y., Xin, K., Shi, B., Wang, R.C., Chen, J., Gao, W., Shi, P., Fan, C.H., Zhao, C.C., Tian, H., 2018. Angew. Chem. Int. Ed. 57, 3626–3630.
Xu, T.L., Scafa, N., Xu, L.P., Zhou, S.F., Al-Ghanem, K.A., Mahboob, S., Fugetsu, B., Zhang, X.J., 2016. Analyst 141, 1185–1195.
Yang, D.M., Ma, P.A., Hou, Z.Y., Cheng, Z.Y., Li, C.X., Lin, J., 2015. Chem. Soc. Rev. 44, 1416–1448.
Yue, X.X., Zhu, Z.Y., Zhang, M.N., Ye, Z.Q., 2015. Anal. Chem. 87, 1839–1845.
Zeng, J.B., Li, M., Liu, A., Feng, F., Zeng, T., Duan, W., Li, M.M., Gong, M.F., Wen, C.Y., Yin, Y.D., 2018. Adv. Funct. Mater. 1800515.
Zhang, K., Zhang, J., Xi, Z., Li, L.Y., Gu, X.X., Zhang, Q.Z., Yi, L., 2017a. Chem. Sci. 8, 2776–2781.
Zhang, Y., Shen, H.Y., Hai, X., Chen, X.W., Wang, J.H., 2017b. Anal. Chem. 89, 1346–1352.
Zhang, Y., Tang, Y.R., Liu, X., Zhang, L.C., Lv, Y., 2013. Sens. Actuators, B 185, 363–369.
Zheng, W., Huang, P., Tu, D.T., Ma, E., Zhu, H.M., Chen, X.Y., 2015. Chem. Soc. Rev. 44, 1379–1415.
Zhou, Y., Chen, W.Q., Zhu, J.X., Pei, W.B., Wang, C.Y., Huang, L., Yao, C., Yan, Q.Y., Huang, W., Loo, J.S.C., Zhang, Q.C., 2014. Small 10, 4874–4885.